



Graphene oxide as a nanocarrier for gramicidin (GOGD) for high antibacterial performance

Journal:	<i>RSC Advances</i>
Manuscript ID:	RA-ART-07-2014-007250.R1
Article Type:	Paper
Date Submitted by the Author:	31-Aug-2014
Complete List of Authors:	Abdelhamid, Hani; NSYSU, chemistry department Khan, Shawan; Marine Biotechnology, Wu, Hui Fen; National Sun Yat-Sen University,

Graphene oxide as a nanocarrier for gramicidin (GOGD) for high antibacterial performance

Hani Nasser Abdelhamid^{1,2}, M. Shahnawaz Khan⁵, Hui-Fen Wu^{1,3,4,5,6*}

¹Department of Chemistry, National Sun Yat-Sen University, Kaohsiung, 804, Taiwan

²Department of Chemistry, Assuit University, Assuit, 71515, Egypt

³School of Pharmacy, College of Pharmacy, Kaohsiung Medical University, Kaohsiung, 800, Taiwan

⁴Center for Nanoscience and Nanotechnology, National Sun Yat-Sen University, Kaohsiung, 804, Taiwan

⁵Doctoral Degree Program in Marine Biotechnology, National Sun Yat-Sen University and Academia Sinica, Kaohsiung, 80424, Taiwan

⁶Institute of Medical Science and Technology, National Sun Yat-Sen University, Kaohsiung, 804, Taiwan

*Corresponding author. Phone: 886-7-5252000-3955. Fax: 886-7-525-3908.

E-mail: hwu@faculty.nsysu.edu.tw

Contract/grant sponsor: National Science Council (NSC), Taiwan

Abstract

As a powerful and novel nanocarrier, graphene oxide (GO) is applied to load a water insoluble antibacterial drug, gramicidin (GD), for effective antibacterial treatments. The loaded amount of GD on the surface of GO was calculated and it was 14% (wt%). Antibacterial activity of GO modified GD (GOGD) was measured against *Pseudomonas aeruginosa* and *Staphylococcus aureus* using plate counting, optical density (OD₆₀₀), transmission electron microscopy (TEM), fluorescence (2D, 3D) and matrix assisted laser desorption/ionization mass spectrometry (MALDI-MS). Use of multiple analytical approaches adds confidence to cytotoxicity assessments of GOGD which showed highly efficiency over than GO and GD. GOGD has the potential wide-ranging effects against different bacteria strains. Nano-cytotoxicity mechanism was discussed in details and previous results controversies were refuted.

Keywords: graphene oxide, gramicidin, antibacterial, fluorescence, mass spectrometry, nanocarrier

Introduction

New antibacterial materials are very important for daily life and for effective health protection. In recent years, conventional organic antibiotic therapies ¹ were becoming less efficient owing to resistant, thermal decomposability, methaemoglobin, cannot use for painting or coating some of them are carcinogens. Thus, applications of nanomaterials as new antibacterial agents have been raised ² and their prevalence in our world is undeniable. Nanomaterials display high antibacterial efficiency, high thermal stability, and can be modified to achieve high selectivity ². The growing interest of nanomaterial in medicine is due to the remarkable properties such as small size, large surface area, simple functionalization, and high activities ³.

Graphene (G) and their derivative (such as graphene oxide, GO) are a honeycomb carbon nanomaterial member that was received enormous potential for biomedical applications included drug carriers ⁴, biosensing ⁵, cancer therapies ⁶ and antimicrobial property ⁷ and become a shining star in the material science in a very short time. The latest progress of using G for various biomedical applications, including antibacterial activities, drug delivery, cancer therapies and biosensing was reviewed ⁸. G and their derivatives such as GO can inhibit the growth of bacterial cells via damage bacterial cell membranes with their extremely sharp edges ¹⁰. G has been combined with nanomaterials to improve their antibacterial activity [¹¹]. G was also conjugated with organic antibiotics in order to increase its antibacterial activity, included heparin–benzalkonium chloride ¹², quaternary phosphonium salt ¹³, lanthanum (III) ¹⁴, chitosan ¹⁵, benzylpenicillin (BP) ¹⁶, polymer [¹⁷, Tween ¹⁸, textile fabrics ¹⁹, peptide ²⁰, and chlorophenyl

²¹. G composites offer high antibacterial efficiency due to the synergistic effect of G and nanoparticles/organic antibiotic.

Gramicidin (GD) is a heterogeneous linear polypeptide antibiotic containing D-and L-amino acids with four tryptophan residues ²². The major challenge of GD is the solubility which limits its antibacterial activity. Furthermore, it has problem related to the development of microbial resistance, surface coating difficulties, cause hemolysis, and relatively high decomposability makes this peptide unsuitable for long-term antimicrobial coatings. Furthermore, therapeutic use of GD is limited to topical application for the treatment of infections from superficial wounds, as it induces hemolysis due to cysteine residues, so it cannot be administered internally. Therefore, the analogs of gramicidin such as GS, that possess additional amino groups with cyclic structure, are active against both gram-positive and gram-negative bacteria ²³.

Herein, we investigated the antibacterial activity of GO materials modified GD (GOGD) against *Pseudomonas aeruginosa* and *Staphylococcus aureus*, which are common bacteria that can cause disease in human. The antibacterial activity of GO nanosheets modified GD against bacteria was investigated by wide range of analytical tool. Data revealed high activity of GOGD and the interactions were discussed intensively.

Chemical and methods

Sulfuric and nitric acids were purchased from J.T. Baker (India). Sinapinic acid (3-(4-hydroxy-3,5-dimethoxyphenyl) prop-2-enoic acid) and natural graphite (-20+84 mesh, 99.9%) were purchase from Alfa Aesar (Great Britain). Gramicidin from *Bacillus aneurinolyticus* (*Bacillus brevis*) was purchased from Sigma-Aldrich (CAS Number 1405-97-6, USA). Methanol (HPLC

grade) and potassium permanganate were purchased from Merck (USA). The de-ionized water obtained from a Milli-Q Plus water purification system (Millipore, Bedford, MA, USA) was used for all experiments.

Instruments

Transmission electron microscopic (TEM) observations were performed on a Philip CM-200, Switzerland. TEM was operating at an accelerating voltage of 100 kV. The samples were prepared by placing a drop of homogeneous suspension on a copper grid and allowing it to dry in air. Fourier transform infrared (FT-IR) spectra were recorded on Perkin-Elmer Spectrum over wavenumber range of 450-7800 cm^{-1} . UV-visible spectroscopy (Lambda 25) with a quartz cell (1 cm) was carried out to characterize the optical properties of the synthesized nanomaterials. Origin V 6.0 was used to analyze the experimental data and draw the graphs. X-ray diffraction (XRD) has measured by Bruker AXS D8 Advance, German. The fluorescence spectra were performed in a fluorescence spectrophotometer (F-2700 Hitachi Co., Japan), equipped with a xenon arc lamp (150 W). The scan speed was set at 120 nm min^{-1} . Matrix assisted laser desorption/ionization mass spectrometry (MALDI-TOF-MS) spectra were obtained from Microflex (Bruker Daltonics, Bremen, Germany) equipped with a nitrogen (N_2) laser (wavelength 337 nm). The spectra were recorded in positive and linear mode using an acceleration voltage of 20 kV and 10 ns extraction delay time. Sinapinic acid was used as a matrix for all experiments.

Experimental part

Preparation of graphene oxide (GO)

GO was synthesized according to our previous publication ²⁴ which based on the Hummers method. Briefly, in a round flask contain natural graphite (1 g) was placed in an ice-bath (with

sodium chloride), which was then subjected to magnetic stirring (Ciramec). After that nitric acid (10 mL, 69-72%) was added into the flask, Sulfuric acid (15 mL, 96.0%) and subsequent potassium permanganate (3 g, $\geq 99\%$) were added gradually into the mixture. The temperature was kept $< 0\text{ }^{\circ}\text{C}$ by using ice-sodium chloride bath. After removing the ice-bath, the hydrogen peroxide (30-32%, 15 mL) was added drop wisely to remove the excess of permanganate (till bubbles stop). After magnetic stirring for 2h, distilled water (200 mL) was poured slowly into the mixture to obtain a dark brown colloidal suspension. Further stirred for another 30 min, the dispersion was filtered then washed several times with a 5 wt% HCl solution to remove metal ions.

Preparation of graphene oxide@gramicidin (GOGD)

About 1 g of GO has dispersed into 50 mL de-ionized water. About 200 mg of GD dispersed and stirred for 24h till completely dispersed. The prepared material were centrifuged and then re-suspended in water. The concentration of GD loaded on GO was determined by the external standard calibration using MALDI-MS and it was 14% (wt/wt).

Preparation of GD solution

GD solution was prepared by the same amount which loaded in GO i.e 14% using methanol as solvent.

Bacterial Culture

Staphylococcus aureus (BCRC 10451) and *Pseudomonas aeruginosa* (BCRC 10303) standard cultures were purchased from Bioresource Collection and Research Center (Hsin-Chu, Taiwan) and were cultivated at $37\text{ }^{\circ}\text{C}$ and maintained on DifcoTM Nutrient broth (Becton and Dickinson, France, 8g per 1 L) and Agar plates (Gen Chain Scientific , GCS, New York, USA, with 1.5%

agar). Both bacteria cells were grown individually overnight at 37 °C using agar medium and then harvested via noodle then re-suspended in sterile de-ionized water (1 mL).

Antibacterial assay using optical density

Before each experiment, all utensils were autoclaved at 120 °C for 20 min to ensure sterility. Gram-negative “*P. aeruginosa*” and Gram-positive “*S. aureus*” were cultured in agar plate for 24 h at 37 °C reach a stationary growth phase. To examine the bacterial inhibition in the presence of various nanomaterials, *P. aeruginosa* and *S. aureus* cells (further diluted to a starting concentration around 2.9×10^{11} and 2.8×10^{11} cfu/mL, respectively) suspended in 1 mL deionised water after addition of different doses of GD, GO and GOGD (0.25, 0.50, 0.75 and 1 mg/mL). Inhibition rate and bacterial concentrations were determined by measuring the samples’ optical densities (OD) at 600 nm. Dilution (3 fold) of a sample would be needed if the optical density exceeded the measurement capability of the spectrometer.

Antibacterial assay using plate count protocol

To examine the bacterial inhibition in the presence of various nanomaterials, *P. aeruginosa* and *S. aureus* cells (5.50×10^{11} and 5.72×10^{11} cfu/mL, respectively) suspended in 1 mL deionised water after addition of different doses of GD, GO and GOGD. The number of target organisms present in the sample was determined by surface plating 0.1 mL of *P. aeruginosa* and *S. aureus* dilutions on agar (Difco Laboratories). After incubating at 37 °C for 24h; the presence of the organisms was confirmed by the color of the colonies on the media; *S. aureus* was golden; while *P. aeruginosa* was blue-green on agar.

For minimum inhibition concentration (MIC) determination, 50 mL of 1/10,000 dilution of overnight culture of bacteria in agar media was added to different vials. The vials were incubated

at 30 °C for 20 h, and MIC was determined by visual assay as the lowest concentration resulting in complete inhibition of growth after inoculation in agar medium.

Fluorescence spectroscopy measurements

In order to probe the interactions among GD, GO and GOGD, fluorescence emission of tryptophan was measured at excitation wavelength 295 nm. *P. aeruginosa* and *S. aureus* cells (2.9×10^{11} and 2.8×10^{11} cfu/mL, respectively) suspended in 1 mL deionised water were incubated with different doses of GD, GO and GOGD (0.25, 0.50, 0.75 and 1 mg/mL) then measured directly after vortex.

Transmission electron microscopy (TEM) imaging

Bacterial cells were first collected from agar plate by centrifugation at 10000 g for 10 min, and the bacterial pellets were washed three times with sterilized deionized water to remove residual culture media. The bacteria *P. aeruginosa* and *S. aureus* cells (1 mL contains 5×10^8 and 8×10^7 cfu/mL, respectively) were treated with GD, GO, and GOGD (1 mg/mL) for 30 min. Then the bacterial cells were fixed with 2.5% glutaraldehyde for 30 min firstly, after washed twice with deionised water, the cells were fixed with 1% osmium tetroxide for 30 min. After fixation, 10 μ L of a sample drop was spotted onto a copper grid-supported carbon film. TEM imaging was performed on a Philip CM-200 field emission transmission electron microscope with an acceleration voltage of 200 kV.

Matrix assisted laser desorption/ionization mass spectrometry (MALDI-MS)

For MALDI-MS analysis the bacterial *P. aeruginosa* and *S. aureus* cells (1 mL contains 5×10^8 and 8×10^7 cfu/mL, respectively) were treated with GD, GO and GOGD (1 mg/mL) for 30 min. About 10 μ L of a sample drop were mixed with 10 μ L of sinapinic acid matrix (50 mM, 50:50,

ACA: H₂O). Then 2 μ L of the mixture were spotted in MALDI target plate and kept for drying before MALDI analysis.

Results and Discussion

Graphene oxide (GO) has attracted great attention due to its excellent water dispersity and amphiphilic behaviors²⁵. Thus, GO sheets demonstrate the strongest antibacterial activity among several G nanomaterials⁸. GO has been applied intensively in nanomedicine because it has two sides that has high capacity to load with the drugs and easy to modify. Furthermore, it contains several kinds of oxygen functional groups, such as hydroxyl, epoxide, carbonyl, and carboxyl groups, on its basal planes and edges, which assist functionalization with peptide such as GD. Based on that, our main purpose of this study is to solve the solubility limitation of GD using GO as a nanocarrier.

Characterization of GOGD

Among the different methods which used to prepare GO, Hummers method is facile and scalable approach²⁴. GO has been characterized using TEM, SEM, EDX, mass spectrometry, UV, FTIR and fluorescence. TEM image (Fig.1 (A-B)) of GO and GOGD shows a clear and transparent nanolayer sheet. It shows a large nanosheets (619 nm) with width 1nm. Carbon nanomaterials such as G is rich by π -bonds, thus it offer a continuous UV absorption with maximum absorption at 295 nm as shown in Fig.1C. Due to this feature, G has been working for excellent photothermal properties upon near infrared (NIR) laser irradiation using glutaraldehyde²⁶ or antibody²⁷ that capture the bacteria and enhance antibacterial activities. GD shows absorption at 250 nm Fig.1C. Fourier transform infrared (FTIR) of GD and GOGD were reported (Fig.1D). GD (Fig.1D) displays peaks at 3750,

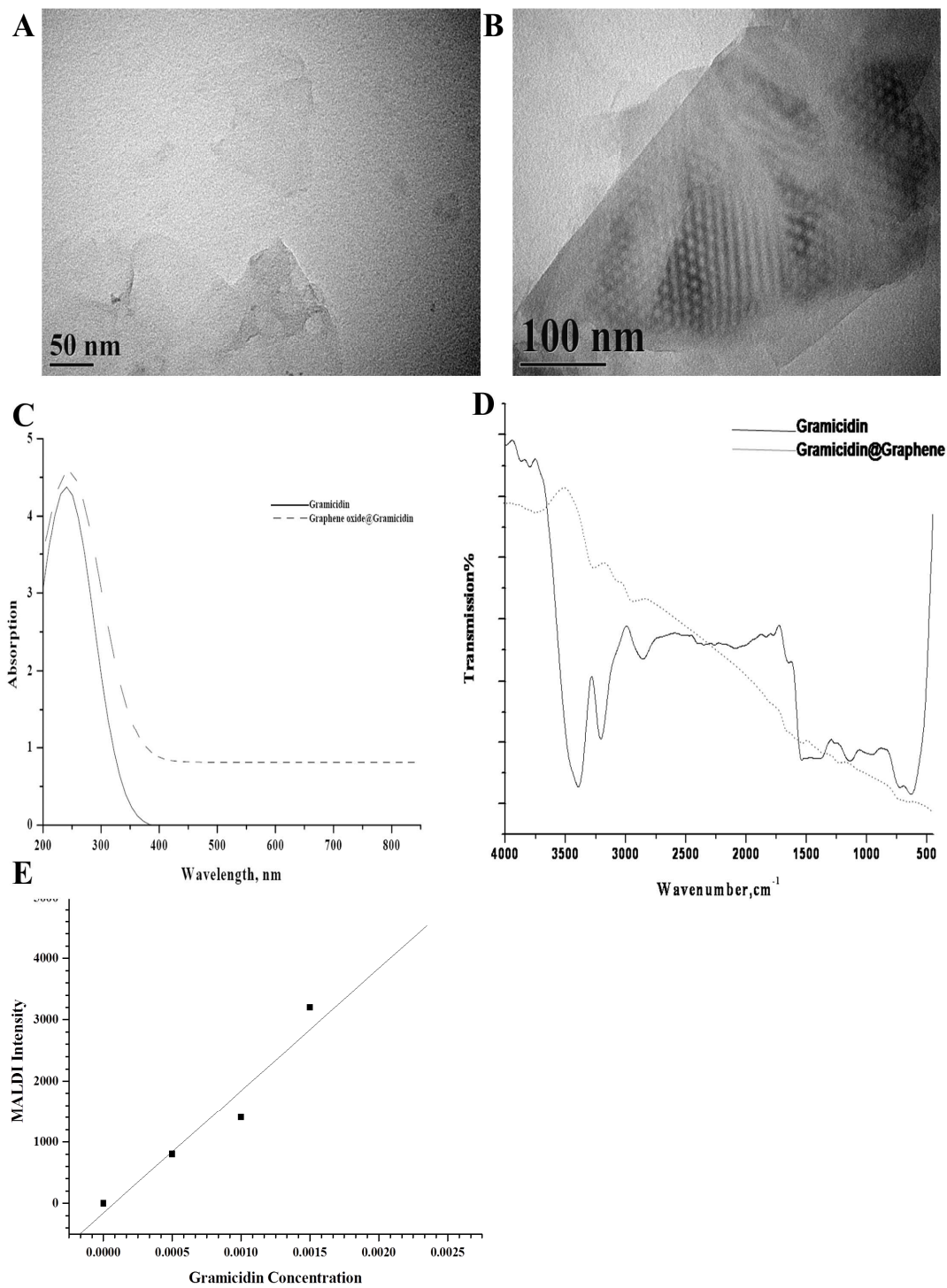
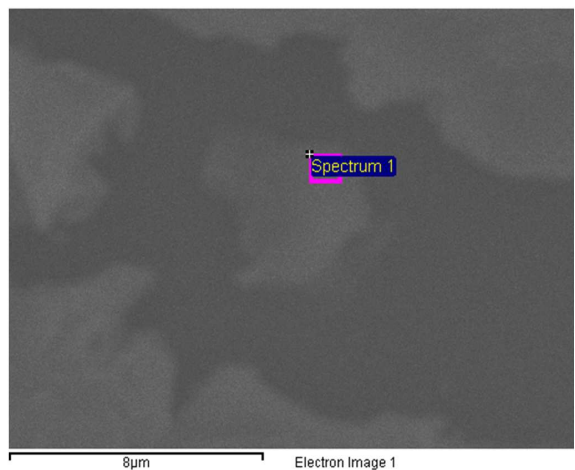


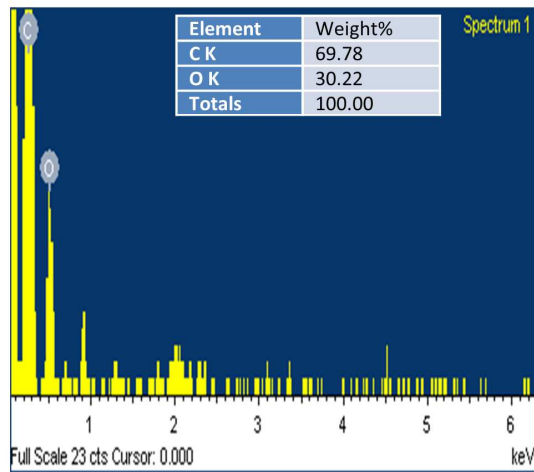
Figure 1. Characterization of GO and their derivative (GOGD) using TEM for (A) GO and (B) GOGD, (C) UV, (D) FTIR, (E) calibration curve using MALDI-MS

3450, 3125, 2750, 1715 and 1150 cm^{-1} corresponding to N-H, O-H, C-H, C-H (stretch), C=O, and C-O, respectively. GO contains hydroxyl, epoxy and carboxyl functional groups on its plane and edge, thus it is able to dispersed in water. GD vibration bands were shifted to 3700, 3250, 3100, 2800, 1700, and 1510 cm^{-1} , respectively after modified with GO (Fig.1D). FTIR reveals that there are strong interactions between GD and GO. To evaluate the GD amount which loaded of GO, MALDI has been investigated. MALDI-MS is a powerful technique to detect and identify peptide and other biomolecules ²⁸. Generally, ionization of peptides enhanced in presence of nanomaterial such as G due to high surface area ²⁶. In order to evaluate the concentration of GD on GO, an external calibration curve has been used Fig. 1F. MALDI spectra (Fig.S1) shows peak at 1882 Da which assigned as $[\text{GD}+\text{H}]^+$ corresponding to the major component i.e gramicidin A (Fig.S1). GD adducts with inorganic monovalent cations can produce ions at m/z 1905.0, 1921.0, 1936.7 Da, that were $[\text{GD}+\text{Na}]^+$, $[\text{GD}+\text{K}]^+$ and $[\text{GD}+\text{K}+\text{H}_2\text{O}]^+$, respectively ²⁹. From calibration curve (Fig.1F), the loaded amount of GD is 14% (wt/wt). As a rule of thumb, increase the bulk structure of the drug, as here i.e GD, decrease the drug loading capacity which may be due to the steric hindrance effect of the loaded molecule ^{4, 28}. To evaluate the antibacterial activity of GO, GD, and GOGD, solution of GD with the same concentration has been prepared (14%). The morphology and elemental analysis for GOGD were measured using SEM (Fig.2A) and EDX (Fig.2B), respectively. SEM (Fig.2A) shows the plate structure of GOGD. While elemental analysis show it is mainly contain C and O. However, the EDX is not appropriated for light element such C or O, but we carried it to confirm the absence of any metals that can cause cytotoxicity. It is very important to throw the light on the forces that govern GD-GO interactions. GO is multifunctional material, it can load peptides through the stacking interactions via the large hydrophobic basal plane of GO with aromatic

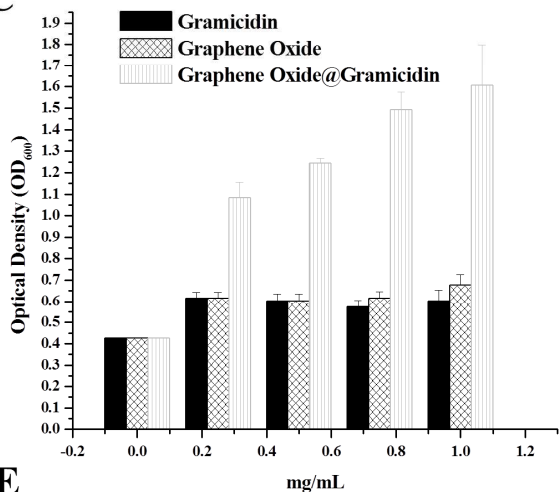
A



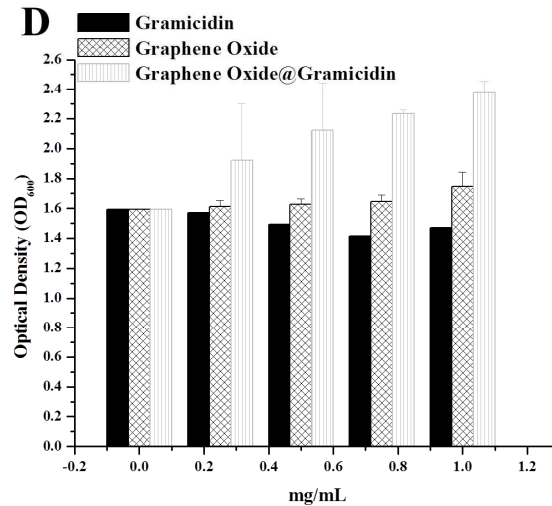
B



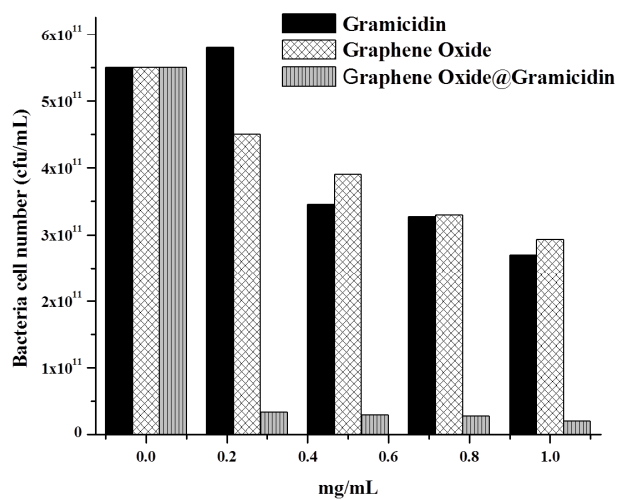
C



D



E



F

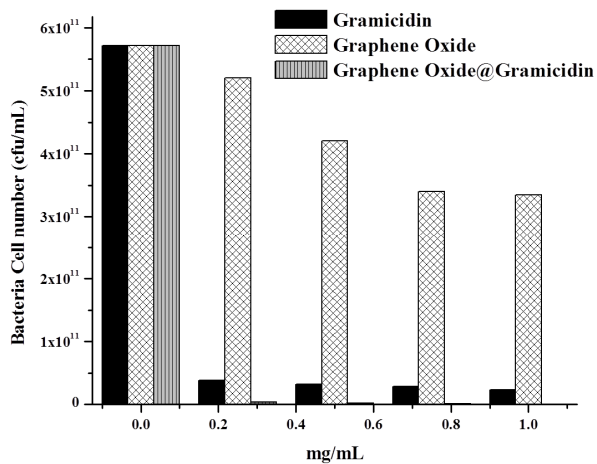


Figure 2. (A) SEM and (B) EDX analysis for GOGD, Biological activity of GD, GO, and GOGD using optical density (OD_{600}) and plate counting. Optical density (OD_{600}) for *P. aeruginosa* (C) and *S. aureus* (D), and plate counting *P. aeruginosa* (E) and *S. aureus* (F)

amino acids and the hydrophobic portion of GD^{6, 30}. GO can also interact via the electrostatic interactions of its ionizable edges with cationic charge of GD. The material i.e GOGD is stable for at least one month without any further aggregation or agglomeration.

Antibacterial activity

The antibacterial activities of cationic peptide (GD), GO and GOGD were investigated using *P. aeruginosa* and *S. aureus* as a model pathogen. Pathogenic bacteria such as *P. aeruginosa* and *S. aureus* are serious bacteria for human health. Thus discover new antibacterial materials are very important for daily life and for effective health protection. GD acts by either making the plasma membrane of bacteria more permeable to essential ions or by inhibiting cell wall synthesis²³. It caused rapid depolarization of the bacterial cytoplasmic membrane that resulted in rapid killing²³. In order to evaluate the antibacterial activities of GD, GO and GOGD, we used two different techniques; plate counting and optical density (OD_{600}).

The optical density, was measured at 600 nm (OD_{600}), indicates the density of bacteria. Optical density (OD_{600}) of *P. aeruginosa* (Fig.2C) and *S. aureus* (Fig.2D) reveals antibacterial activities of GD, GO and GOGD. As shown in Fig.2 (C-D), there is increase in optical density with increase nanomaterials concentration (0.5-1 mg/mL). The increment of optical density may be reveal cytotoxicity of nanomaterials. However, Ruiz. et.al.³¹ also report increase in optical density of bacteria when it incubated with GO and they concluded that due to nonspecific

enhancer of bacteria growth in nutrient broth. So that we suspend the bacteria in sterilized and deionized water which can give a clear background than nutrient broth as it may be cause also turbidity during OD₆₀₀ measurements. Furthermore, increase optical density may be due to intrinsic absorption of GO as previous shown in Fig.1C^{26-27 56-57}. So that we subtracted the intrinsic value of OD₆₀₀ for GO at these concentration. Thus, the OD₆₀₀ is only function on the bacteria concentration. It was reported that G-based nanomaterials materials can oxidize glutathione, which serves as redox state mediator in bacteria^{7b 14}. Because of the membrane and oxidation stress, optical density may be display increment^{7b 14}. When bacteria cells deposit on GO or GOGD nanosheets, the sharp edge of GO nanosheets may cause significant membrane stress. GO derivatives (GO and GOGD) are a few nanometer, thus it serves as “Knife” which can disrupt and damage cell membranes, leading to the release of intracellular contents, and eventually increase optical density. In general, GO offers the higher antibacterial activity among the different G-based nanomaterials. Data reveal high activity in order GOGD > GO ≥ GD. Results indicate a trivial increase of GD and GO with increase the concentration. In contrast, GOGD offers a significant increase in optical activity that reveals higher cytotoxicity. Optical density (Fig.2C-D) reveals high cytotoxicity of GO, and GOGD toward *P. aeruginosa* over than *S. aureus*. Indeed, *S. aureus* (Gram-positive) bacterium with thick peptidoglycan (20-80 nm), without an outer membrane. In other side, *P. aeruginosa* (Gram-negative) bacterium has a much thinner layer of peptidoglycan (thickness of 7-8 nm) beside a layer of lipopolysaccharides layers which can interact hydrophobically with GO³³. These factors are the main reason why nanomaterials display high antibacterial activities toward *P. aeruginosa* over than *S. aureus*. A similar study has shown that contact of *E. coli* and *S. aureus* bacterial cells with GO can cause growth reductions of about 51 and 61%, respectively^{7c}. This discrepancy may be due to different

respond of *E. coli* and *P. aeruginosa*^{7c 16}. Furthermore, the antibacterial assessments are different. The minimum inhibitory concentrations (MIC) of these materials against the different bacteria were tabulated in Table S1 (supporting information file). To address this issue, we characterize the antimicrobial properties of GO, GD, and GOGD using plate counting protocol (Fig.2(E-F)). It can be observed that more and more bacteria were killed with increase concentration of nanocomposites (GOGD). Data reveal high toxicity of GOGD over than GD and GO. Optical photograph of plate counting were reported for *P. aeruginosa* (Fig. S2(A-D)) and *S. aureus* (Fig.S3(A-D)). Images indicate high bacteria eradication in order GOGD>GO>GD. However, optical density (OD₆₀₀) and plate counting are different analytical techniques, but they reveal cytotoxicity of the nanomaterials. To solve the discrepancies between plate counting and optical density, we should take in our consideration the different in the principle and accuracy of both techniques. Optical density was based on turbidity while plate counting was based on count the cell after growth on agar plate. Because both technique were measure at different time (30 min for OD₆₀₀ and after 24h incubation for plate counting), thus they may be give different results. It is also noted that during the growth of bacteria on agar plate, nanomaterial was incubated with the bacteria cells that implies long exposure. Kawai and coworkers reported that gramicidin S (GS) is inactive or only moderately active against gram-negative bacteria while it is strong against gram-positive as reported here²³. They claimed that due to the outer membrane of gram-negative bacteria prevents the penetration of hydrophobic antibiotics into cells, which explains the low activity of GS against gram-negative bacteria.

GD as an antimicrobial agent has been limited due to its poor solubility, thus it is soluble in methanol that display self-toxicity only to the bacterial cells but also for mammalian cells. The incorporation of GD in GO is an effective and alternative way of improving their dispersion in

aqueous medium. Generally, the dispersion of GD on GO depends on the functional groups on GO nanosheets. Due to the carboxyl, hydroxyl, and epoxy groups are introduced on GO sheets, it can form much more stable dispersions with GD. Beside that GO has multi-functions, thus it controlled release of the antibiotic by various routes such as membrane acidity. GOGD can form stable dispersions antibacterial nanocomposite, thus offers more opportunities to interact with cells that enhance the bacteria killing activities. This interaction is not useful only to increase dispersibility, but can also use to control and sense drugs based on dynamic bonding interactions (such as, hydrogen bonding, hydrophobic, p-p stacking and electrostatic interactions)³³. Pendey et.al³⁴ demonstrated the controlled release behavior of water soluble drug called gentamicin sulfate from G nanosheets. They revealed that gentamicin released from the G nanomatrix showed a better fit with the Korsmeyer–Peppas model ($R^2= 0.99, 0.98, \text{ and } 0.99$ at pH 3, 7.4 and 9 respectively)³⁵. Drug was released in different pH in order that: acidic (pH 3) > basic (pH 9) > neutral (pH 7.4). Thus, GD was released from GOGD when it reaches the bacteria cell membranes based on their acidity. However, the situation is quite complicated here as pH of the cell membrane is unknown to us and GD can overlap with the proteins of bacteria cells. It was reported that G can destroy DNA and RNA³⁵⁻³⁶.

Fluorescence spectra

We further carried out a fluorescence assay to verify the bacteria survival rate via evaluation the interactions among GD, GO, and GOGD with pathogenic bacteria.

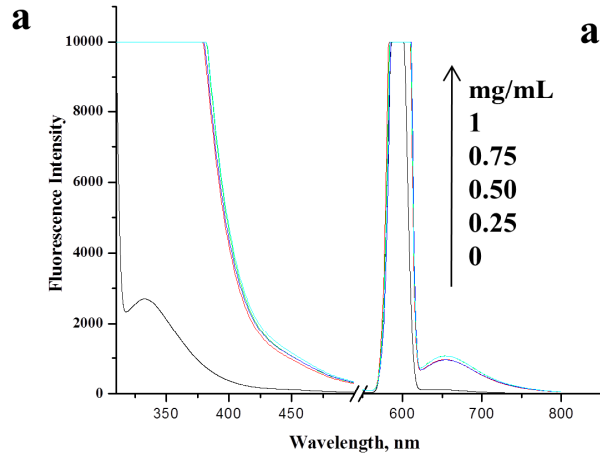
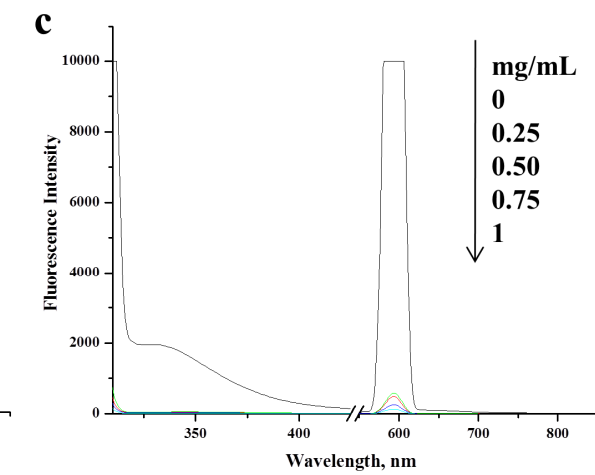
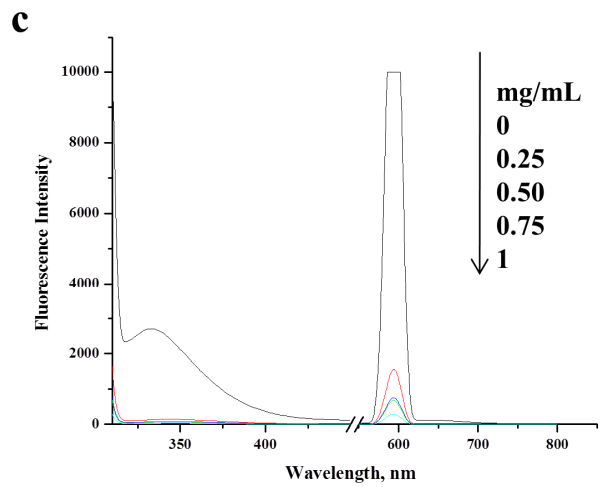
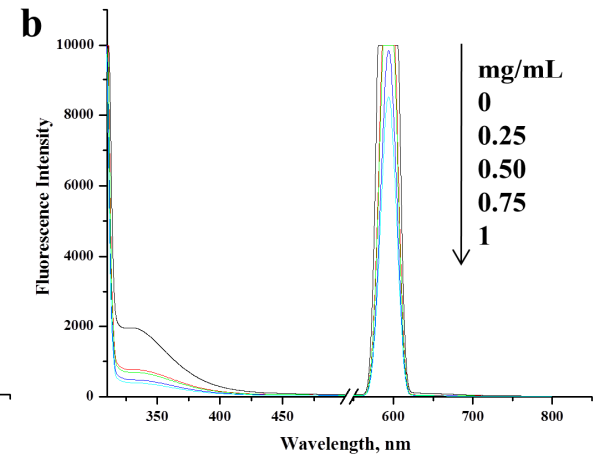
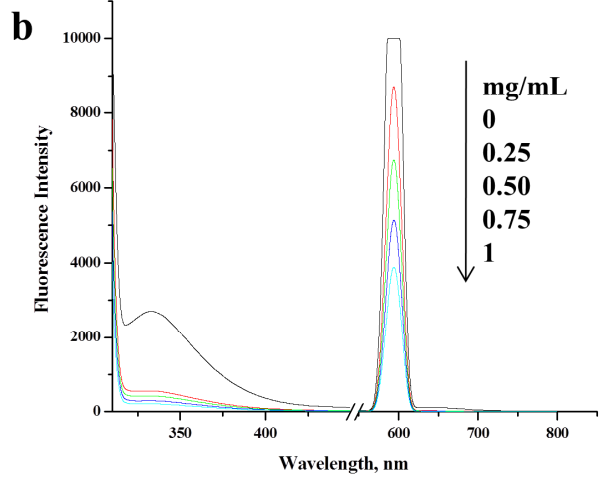
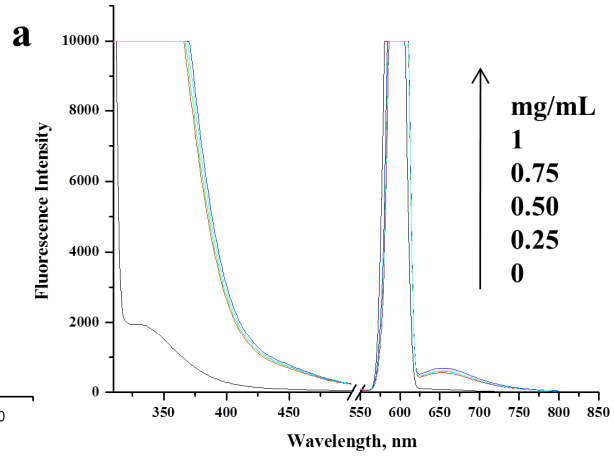
A**B**

Figure 3. Fluorescence emission of tryptophan for (A) *P. aeruginosa* and (B) *S. aureus* after incubation with (a) GD, (b) GO and (c) GOGD

Fluorescence spectroscopy is a powerful tool to study native protein structure and their interactions. Among the different amino acids, building units of proteins, phenylalanine (Phe), tyrosine (Tyr) and tryptophan (Trp) could display fluorescence emission³⁷. At excitation wavelength 295 nm, the main fluorescence emission comes from tryptophan amino acid. Measure the Trp quenching or shifting can be used to evaluate interaction with proteins. Generally, when nanomaterials interact with protein, it displays change in their conformation, thus the emission of Trp will undergoes shift or quenching. Trp emission spectra of *P. aeruginosa* and *S. aureus* were shown in Fig.3. Bacteria proteins show emission peaks at 334 nm corresponding to Trp emission (Fig.3). Because the bacterium *P. aeruginosa* (Fig.3A) and *S. aureus* (Fig.3B) have tryptophan amino acid, they display the same fluorescence emission. GD contains 4 tryptophan amino acids, thus it overlap and enhance of bacteria protein emission (Fig. 3A (a) and Fig. 4B (a)). In contrast GO and GOGD quench the Trp emission with increase nanomaterials concentrations as shown in Fig.3. Data reveals high quenching in case of GOGD over than GO (Fig. S4). Fig.3 indicates high interaction between GOGD over than GD or GO. In comparison between *P. aeruginosa* (Fig.3A) and *S. aureus* (Fig.3B), quenching rate in the former is higher which confirm results of optical density (Fig. S4). In order to confirm the fluorescence results, second (2D, Fig.S5) and third dimension (3D, Fig.4) fluorescence spectroscopy of pathogenic bacteria were reported. *P. aeruginosa* (Fig.4A (a)) and

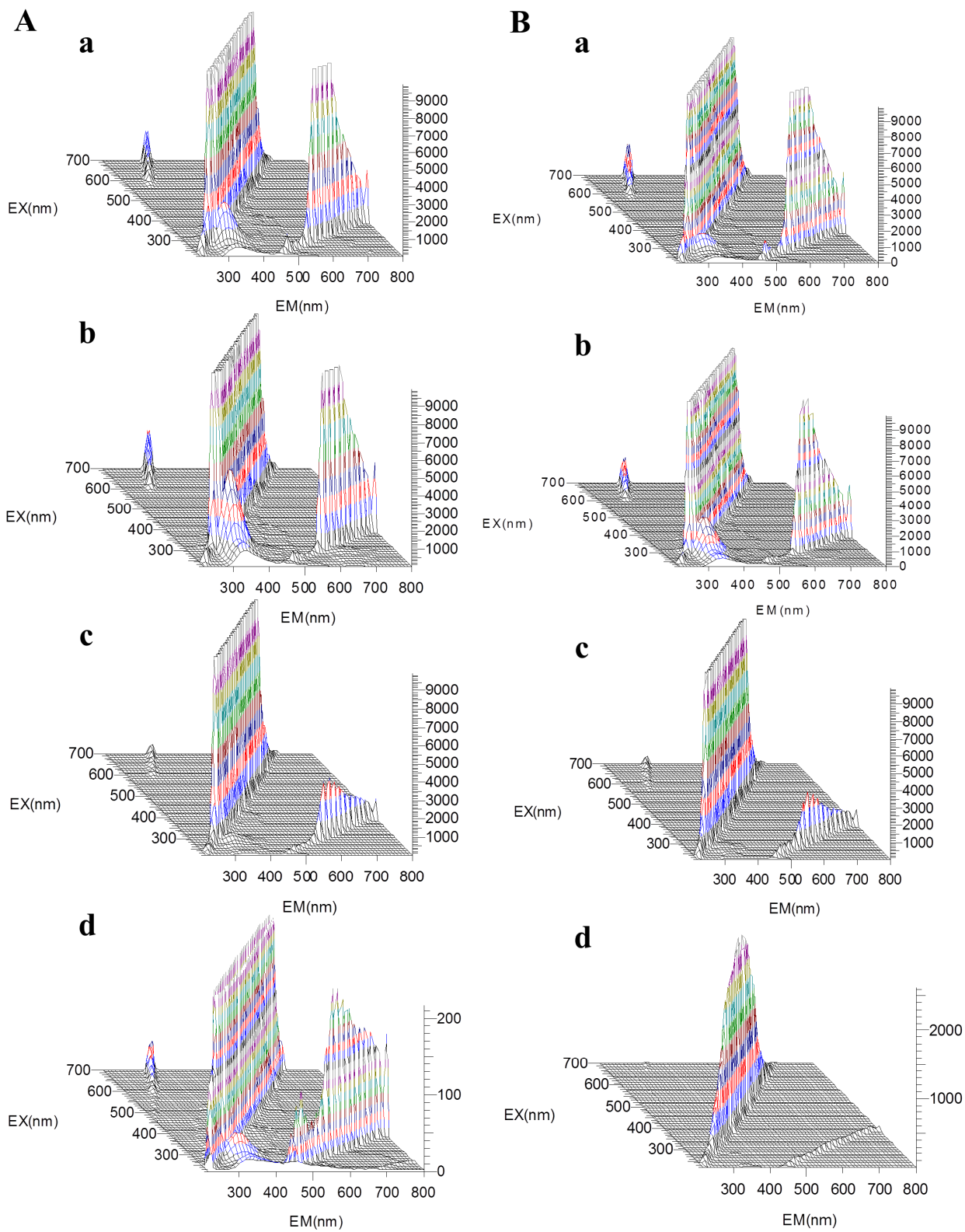


Figure 4. 3D-Fluorescence emission of tryptophan for (A) *P. aeruginosa* and (B) *S. aureus* after incubation with (a) control, (b) GD, (c) GO and (d) GOGD

S. aureus (Fig.4B (a)) display the same pattern as proteins contents are the same. Interestingly, fluorescence spectroscopy gives valuable results because the cytotoxicity of GO was not found to be strongly dependent on the duration of incubation time³⁸. Thus, fluorescence measurements were measured directly after incubation with nanomaterials. Quenching of bacteria protein membranes may be due to the high protein adsorption of GO^{39-41 72-74}. High quenching of Trp indicate that there are interaction among the bacteria and nanomaterial that may be implies cytotoxicity.

Matrix assisted laser desorption/ionization mass spectrometry analysis of the interactions between the bacteria cell and nanomaterials

Among the various analytical tools, MALDI-MS²⁸ receive a massive attention as it can give a direct and clear profile of the bacteria and their change after interaction with various xenomaterials. We measured MALDI-MS profile of pathogenic bacteria i.e *P. aeruginosa* (Fig.5A) and *S. aureus* (Fig.5B) after and before interaction with GD, GO, and GOGD. MALDI may be useful to probe the effect of nanoparticles on the bacteria lysates and clarified the effect of nanomaterials on the bacteria cells lysate. Especially, bacteria cells can be adapt very rapidly to their environment, so MALDI can give a rapid evaluation of the interaction affinities among the bacteria and GD, GO and GOGD. The merit of MALDI over than fluorescence is that MALDI gives a complete profile for the bacteria before and after the interactions. In other side, fluorescence depends on the intrinsic fluorescence of aromatic amino acids i.e tryptophan. The intensities of mass spectral peaks presumably reflect molecular concentrations in the cells due to

the large surface area of nanomaterials. Furthermore, MALDI offer the effect of bacteria on the ionizability of GD. MALDI spectra (Fig.5) reveal a complete change in bacteria lysate after interaction with GD, GO and GOGD. Spectra indicate suppression of bacteria ionization due to interaction with xenomaterials. Surprisingly, GO shows complete suppression of *S. aureus* (Fig.5B (c)) ionization that reveal a strong interactions (adsorption) between GO and cell membranes. This effect was not observed with *P. aeruginosa* (Fig.5 A(c)) due to the difference of thickness and composition of cell membranes. *P. aeruginosa* is rich by lipopolysaccharide (LPS), called also as endotoxin, which can easily cut by the sharp edge of GO. In contrast *S. aureus* miss the layer and has thick layer of peptidoglycan. However, bacteria lysate present in higher concentration over than GD, but the latter still ionized effectively without any suppression. This observation may be indicate that GD conformation display no or low changes in presence of bacteria cells. MALDI results indicate a strong effect of GD, GO and GOGD on bacteria cell lysate. MALDI data showed a significant change in case of nanomaterials (GD, GOGD) over than GD) which implies high toxicity.

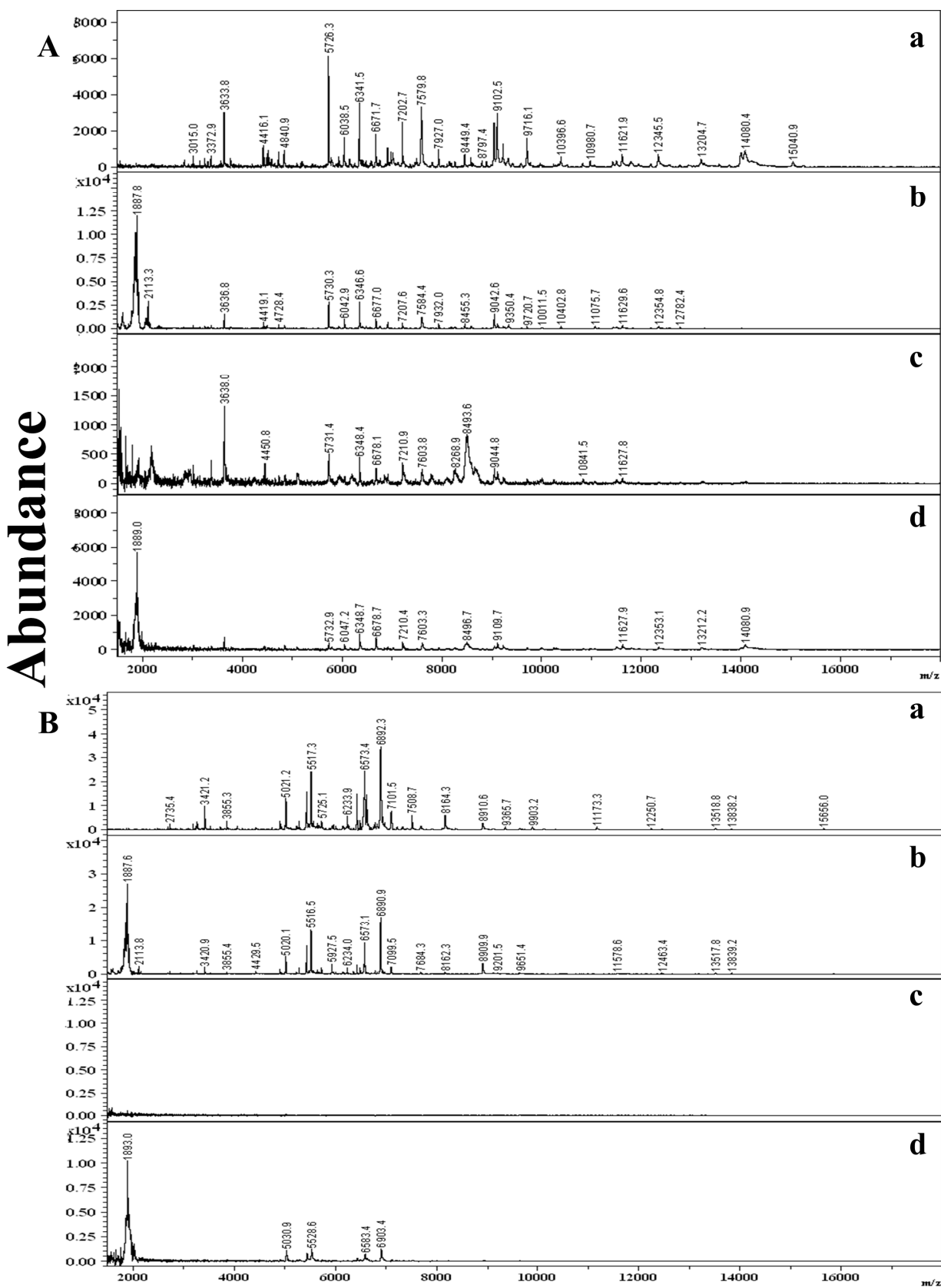


Figure 5. MALDI-MS spectra of (A) *P. aeruginosa* and (B) *S. aureus* after incubation with (a) control, (b),GD (b) GO and (d) GOGD

Cell morphological change with nanoparticle

Transmission electron microscopy (TEM) was employed to evaluate the surface morphology change of the native *P. aeruginosa* (Fig. 6A (a)), *S. aureus* (Fig. 6B (a)) and treated cells with the prepared nanoparticles (GO, GOGD) and antibiotic (GD). *P. aeruginosa* (Fig. 6A (a)) is rod-like shape. After incubation with GD, GO, and GOGD (1 $\mu\text{g}/\text{mL}$) for 30 min, most of the cells displayed a tubular shape with the ends being destroyed, indicating both the outer and inner membranes of the cells were damaged (Fig. 6A).

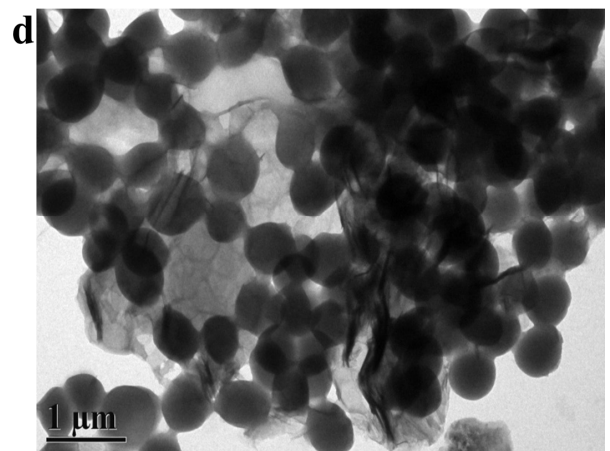
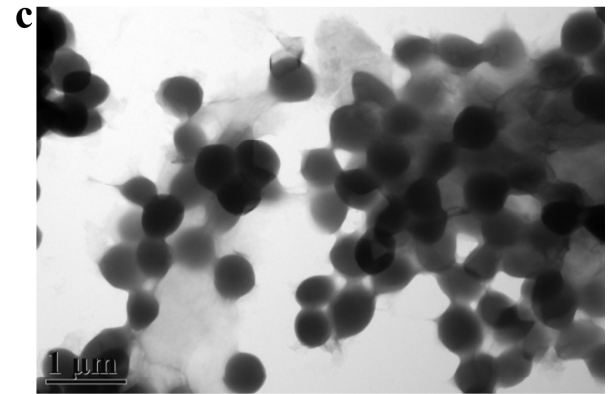
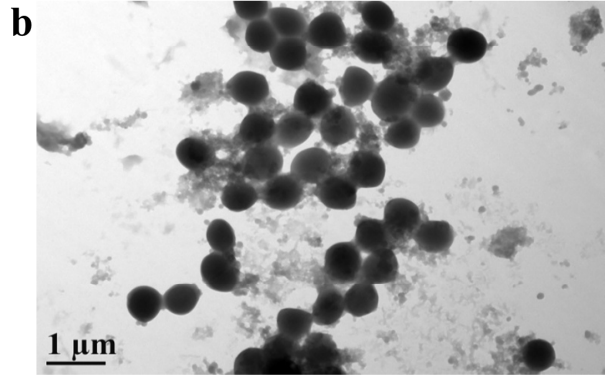
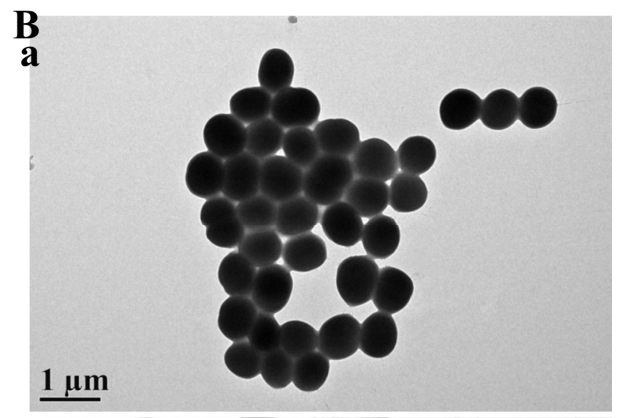
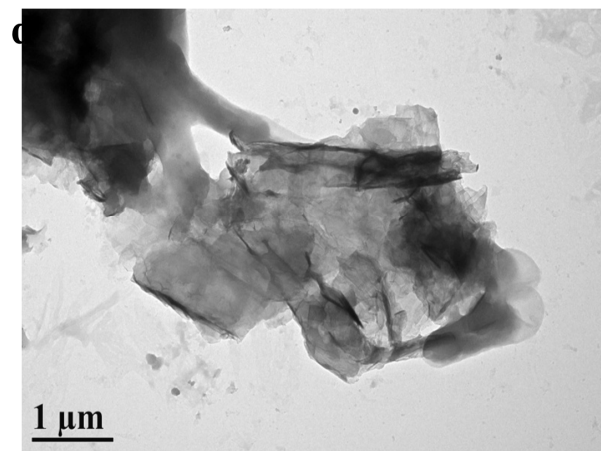
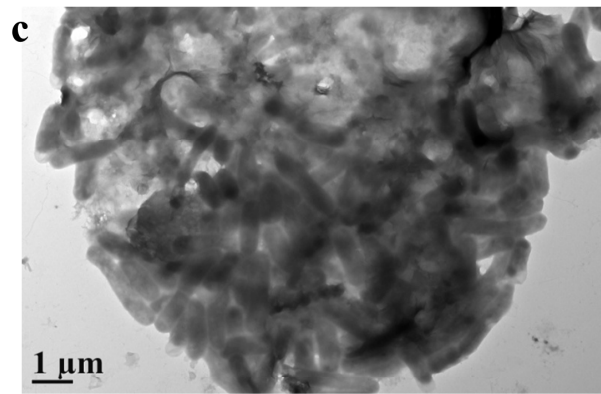
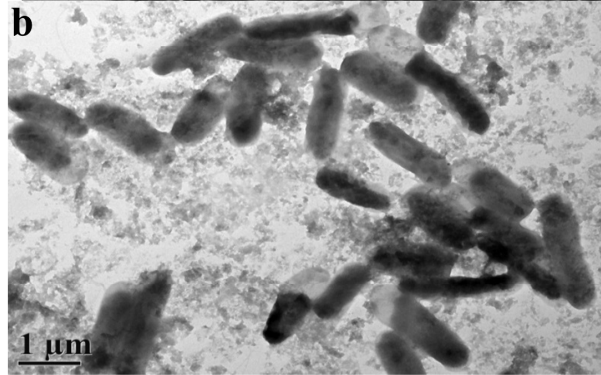
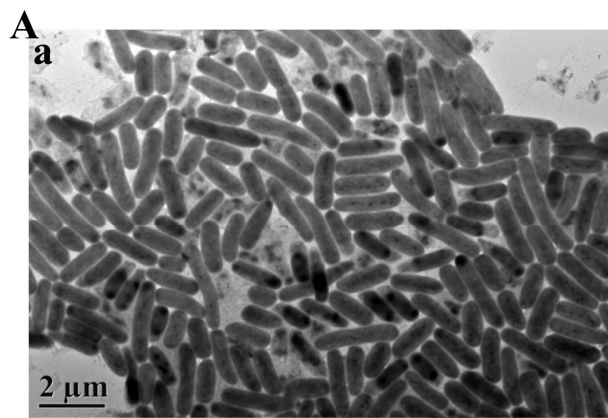


Figure 6. TEM images of (A) *P. aeruginosa* and (B) *S. aureus* after incubation with (a) control, (b) GD, (c) GO and (d) GOGD

S. aureus is Gram-positive coccus, which appears as grape-like clusters (Fig.6B). Most of the *s.aureus* cells displayed destruction for both the outer and inner membranes of the cells (Fig. 6B). TEM images reveals high destroy of the cell morphology in the order to GOGD>GO>GD. The different behavior of GO and GOGD observed in TEM images suggests the aggregation/dispersion of G-based materials may play an important role in their antibacterial activities. GO and GOGD are a few sheets with nanoscale width, thus it serve as “Knife” which can disrupt and damage cell membranes, leading to the release of intracellular contents, and eventually kill the bacteria cells. This effect increase in case of GD due to synergetic effect which based on increase metals impermeability.

Cytotoxicity mechanism

In fact, there are multiple conflicting reports about the biocompatibility and antimicrobial activity of GO. Because of these numerous conflicting reports about the antimicrobial properties of GO, we performed an in-depth characterization of the antimicrobial activity of GO, and GOGD with various analytical tools and protocols such as plate counting, OD₆₀₀, TEM, MALDI, and fluorescence (normal, 2D, 3D). These conundrums appeared due to various factors. First, different bacteria were studied that displayed different and distinctive behavior toward the various nanomaterials. It should be noted that these two different strains differ in both their behavior and responds to the same nanomaterials. Second, cytotoxicity of nanomaterials is dose dependent. For instance recent studies showed that the dose-dependent cytotoxicity of GO during the 24 h incubation time was attributed to the generation of reactive oxygen species (ROS)⁴²⁻⁴³.

Third, agents used during preparation such as capping/stabilizing/dispersive agents play a significant role on GO cytotoxicity. For instance, non-functionalized GO was capable of killing bacteria via cell membrane damage ⁷. Fourth, bacteria can play an influential effect on the nanomaterial. For instance, it was found that *E. coli* ⁴⁴ and *Shewanella* bacteria ⁴⁵⁻⁴⁶ could reduce GO through the bacterial respiration to G that display high toxicity than GO. In other words, GO suspension converted to mixture of GO and G after interaction with bacteria cells. However, G paper has been found to be a biocompatible substrate for adhesion and proliferation of L-929 cells, ⁴⁷ neuroendocrine PC12 cells, oligodendroglia cells, and osteoblasts ⁴⁸. Fifth, size of GO has influential effect on their toxicity. It was found that large GO sheets more easily cover cells, and cells cannot proliferate once fully covered ⁴⁹. In contrast, small GO sheets cannot effectively adhere to the bacterial surfaces ⁴⁹. Thus lateral dimension of GO sheets have important and potential effect on their antibacterial activity. The previous factor may be the reasons why there are discrepancies among the different scientific reports.

In general, antimicrobial properties of carbon-based materials such as carbon nanotube (CNT), fullerenes, GO, and their composite forms against biological systems arise due to physical disruption or oxidative stress ⁵⁰. GO has been employed as an effective nanocargo to deliver water-insoluble GD into the cells. The cytotoxicity of GOGD has suggested three mechanisms; oxidative stress, metal toxicity, and physical disruption causing rupture. Bacteria and the GO nanosheets would repel each other in an aqueous solution due to the negative charge of GO, *P. aeruginosa* (LPS) and *S. aureus* (teichoic acid). However, there are hydrogen bonds among lipopolysaccharide, teichoic acid, lipids, and other subunits in the outer membrane bacteria and oxygenate groups of GO. These forces facilitated the GO nanosheets to adhere bacteria cells then

block the cells from in taking nutrient, and eventually resulting in the cell death. In comparison with GO, a magnificent decrease in negative charge was observed on the GOGD composite due to cationic peptide (i.e GD). It was also reported that the antibacterial mechanism of oxygen-species functional groups was due to the direct contact with the cell walls of bacteria. Furthermore, GD increases metals permeability, thus increase cell death rate. In summary, bacteria have high entrapping due to GO and GD in GOGD. This is in agreement with the previous study ^{7a} in which they demonstrated the inactivation of bacteria by trapping the bacteria between the reduced G and was defined as “capturing-killing process”. The potent antibacterial of GO, and GOGD have been attributed also to membrane stress induced by sharp edges of G nanosheets, thus physical damage to cell membranes, leading to the loss the viability of bacterial cells ⁷. It was found that GO can generate reactive oxygen species (ROS) ⁴⁵ which was proposed as one of the main mechanisms for the cytotoxicity and it function of size ³¹ and concentrations ³². This mechanism may be low probability in case of GOGD because GO has been coated with peptide i.e GD. Sharp edge of GO can also cause antibacterial activities ⁵¹⁻⁵² especially it can intercalate into DNA molecules as reported previously ⁵³. Uncontrolled ion transport across membranes due to GD cause also antibacterial activities as control ion transport is a central feature in many cellular processes such as respiration, nerve conduction, and osmotic homeostasis. However analogy GD shows high activity toward Gram positive and Gram negative, it is still insoluble in aqueous medium and has high hydrophobicity ⁵⁴. Recent computer simulations suggested that GO sheets may destructively extract phospholipids from the bacterial cellular membranes onto their basal planes leading to bacterial death ⁵⁵. A recent study showed that bovine serum albumin and tryptophan undergoes noncovalent adsorption on GO basal planes that account for the deactivation of GO’s bactericidal activity ⁵⁶. They GO

intrinsically kills both bacteria and mammalian cells and noncovalent adsorption on its basal planes may be a global deactivation mechanism for GO's cytotoxicity. The main advantages of GO is their ability to serve for NIR photothermal treatment where we looking for in the near future ⁵⁷. It is can modify with other biopolymers such as chitosan than can increase their solubility and can work as a carrier for small drugs ^{15, 58}. Recently, G enhances the antibacterial activities of metal oxide (SnO₂) against pathogenic bacterial ⁵⁹. In conclusion, we describe a novel nanocomposite (GOGD) for the highly killing of pathogenic bacteria due to oxidation stress, metals, sharp edges, and increase metals permeability.

Conclusion

In summary, we reported for the first time the use of the gramicidin (GD)-functionalized graphene oxide (GO, called as GOGD) for effective antibacterial activities. We proved that GO can absorb gramicidin (water-insoluble) through physical interactions and thus enhance their activity. The ultimate impact of this work may be its high bacterial activities and in-depth study of antibacterial activity using different analytical approached (plate counting, OD₆₀₀, TEM, MALDI, and fluorescence spectroscopy). Almost all the factors that can cause contradict were discussed. The protein-enriched outer envelope of bacteria cells appears to serve as a main target for the GD, GO and GOGD. This new material may be has a promising future for biomedical application in the near future.

Acknowledgement

The authors are particularly grateful to the Ministry of Science and Technology of Taiwan for financial support.

References:

References:

1. M.B. Israela, Z. Meital. *J. Biomed. Mater. Res., Part A.* 2007, **83**, 10–19.
2. T. Kim, T. Hyeon, *Nanotechnology.* 2014, **25**, 012001-012015.
3. C. Marambio-Jones, E. M. V. Hoek, *J. Nanopart. Res.* 2010, **12**, 1531–1551.
4. L.M. Zhang, J.G. Xia, Q.H. Zhao, L.W.Liu, Z.J.Zhang. *Small.* 2010, **6**, 537–544.
5. (a) J.H. Jung, D.S. Cheon, F. Liu, F.B.Lee, T.S. Seo. *Angew. Chem., Int. Ed.* 2010, **49**, 5708–5711; (b) M. Zhou, Y.M. Zhai, S.J. Dong. *Anal. Chem.* 2009, **81**, 5603–5613; (c) H.N. Abdelhamid, H.F. Wu. *J. Mater. Chem. B.* 2013, **1**, 3950-3961; (d) Y.X. Huang, X.C. Dong, Y.X. Liu, L.J. Li, P. Chen. *J. Mater. Chem.* 2011, **21**, 12358–12362; (e) O. Akhavan, E. Ghaderi, R. Rahighi. *ACS Nano* 2012, **6**, 2904-2916
6. (a) O. Akhavan, E. Ghaderi, H. Emamy, *J. Mater. Chem.,* 2012, **22**, 20626-20633; (b) K. Yang, S. Zhang, G. Zhang, X. Sun, S.T. Lee, Z. Liu. *Nano Lett.* 2010, **10**, 3318–3323; (c) X.X. Ma, H.Q. Tao H, K. Yang, L.Z. Feng, L. Cheng, X.Z. Shi, Y.G. Li, L. Guo, Z. Liu. *Nano Res.* 2012, **5**, 199–212.
7. (a) O. Akhavan, M. Choobtashani, E. Ghaderi, *J. Phys. Chem. C* 2012, **116**, 9653-9659; (b) O. Akhavan, E. Ghaderi, K. Rahimi. *J. Mater. Chem.,* 2012, **22**, 23260; (c) W. Hu, C. Peng, W. Luo, M. Lv , X. Li , D. Li, Q. Huang, C. Fan. *ACS Nano* 2010, **4**, 4317-4323; (d) M. Kalbacova, A. Broz, J. Kong, M. Kalbac. *Carbon* 2010, **48**, 4323-4329; (e) O. Akhavan, E. Ghaderi, M. Shahsavar. *Carbon* 2013, **59**, 200-211.
8. (a) S.B. Liu, T.H. Zeng, M. Hofmann, E. Burcombe, J. Wei, R.R. Jiang, J. Kong, Y. Chen. *ACS Nano.* 2011, **5**, 6971–6980; (b) L, Feng, Z. Liu. *Nanomedicine.* 2011, **6**, 317–324; (c) H.Y. Mao, S. Laurent, W. Chen, O. Akhavan, M. Imani, A.A. Ashkarran, M. Mahmoudi. *Chem. Rev.* 2013,**113**, 3407-3424; (d) J. Liu, L. Cui, D. Losic, *Acta*

- Biomaterialia. 2013,**9**, 9243–9257; (e) B. Amedea, Seabra, A. J. Paula, R. de Lima, O.L. Alves, N. Durán, Chem. Res. Toxicol. 2014, **27**, 159–168
9. O. Akhavan, E. Ghaderi. ACS Nano. 2010, **4**, 5731–6.
10. (a) S. Gurunathan, J.W. Han, A. Abdaldayem, V. Eppakayala, J.H. Kim. Int. J. Nanomedicine. 2012,**7**, 5901–5914; (b) K. Krishnamoorthy, M. eerapandian, L.H. Zhang, K. Yun, S.J. Kim. J. Phys. Chem. C 2012, **116**, 17280–17287
11. (a) O. Akhavan, E. Ghaderi. J. Phys. Chem. C, 2009, **113**, 20214–20220; (b) J. Shen, M. Shi, B. Yan, H.W. Ma, Y.Z.Hu, M.X.Ye. Nano Res. 2010, **3**, 339–349 ; (c) J. Ma, J. Zhang, Z. Xiong, Y. Yong, X.S. Zhao. J. Mater. Chem. 2011, **21**, 3350-3352; (d) W.P. Xu, L.C. Zhang, J.P. Li, Y. Lu, H.H. Li, Y.N. Ma, W.D. Wang, S.H. Yu. J. Mater. Chem. 2011, **21**, 4593-4597; (e) X. Cai, M. Lin, S. Tan, W. Mai, Y. Zhang, Z. Liang, Z. Lin, X. Zhang. Carbon. 2012, **50**, 3407-3415; (f) C. Li, X. Wang , F. Chen, C. Zhang, X. Zhi , K. Wang, D. Cui. Biomaterials 2013, **34**, 3882-3890; (g) T. Kavitha , A.I. Gopalan, K.P. Lee, S.Y. Park. Carbon. 2012, **50**, 2994-3000; (h) M.R. Das, R.K. Sarma, R. Saikia, V.S. Kale, M.V. Shelke, P. Sengupta. Colloids Surf. B. 2011, **83**, 16–22; (g) D.H. Zhang, X.H. Liu, X. Wang. J. Inorg. Biochem. 2011, **105**, 1181–1186; (i) H. Wang, J. Liu, X. Wu, Z. Tong, Z. Deng. Nanotechnology. 2013, **24**, 205102-25111, (j) A. Fonseca de Faria; D. S. T. Martinez, S. M.M. Meira, A. C. Mazarin de Moraes, A. Brandelli, A. G. S. Filho, O. L. Alves, Colloids and Surfaces B: Biointerfaces 2014, **113**, 115– 124
12. (a) N. Meng, S.Q. Zhang, N.L. Zhou, J. Shen. Nanotechnology, 2010, **21**, 185101; (b) N.L. Zhou, N. Meng, Y.C. Ma, X.M. Liao, J. Zhang, L. Li, J. Shen. Carbon, 2009, **47**, 1343–1350.

13. X. Cai, S.Z. Tan, M.S. Lin, A. Xie, W.J. Mai, X.J. Zhang, Z.D. Lin, T. Wu, Y.L. Liu. *Langmuir*, 2011, **27**, 7828–7835.
14. X. Wang, N.Z.J. Yuan, W. Wang, Y. Tang, C. Lu, J. Zhang, J. Shen. *J. Mater. Chem.*, 2012, **22**, 1673–1678
15. B. Lu, T. Li, H. Zhao, L. Li, C. Gao, S. Zhang, E. Xie. *Nanoscale*, 2012, **4**, 2978-2982.
16. Y. Wang, D. Zhang, Q. Bao, J. Wu, Y. Wan. *J. Mater. Chem.*, 2012, **22**, 23106-23113.
17. (a) T.S. Sreepasad, M.S. Maliyekkal, K. Deepti, K. Chaudhari, P.L. Xavier, T. Pradeep. *ACS Appl. Mater. Interfaces*. 2011, **3**, 2643–2654; (b) C.M. Santos, M.C.R. Tria, R. Vergara, F. Ahmed, R.C. Advincula, D.F. Rodrigues. *Chem. Commun.* 2011, **47**, 8892–8894;
18. S. Park, N. Mohanty, J.W. Suk, A. Nagaraja, J.H. An, R.D. Piner, W.W. Cai, D.R. Dreyer, V. Berry, R.S. Ruoff. *Adv. Mater.* 2010, **22**, 1736–1740
19. J. Zhao , B. Deng , M. Lv , J. Li , Y. Zhang , H. Jiang , C. Peng , J. Li , J. Shi , Q. Huang , C.Fan , *Adv. Healthcare Mater.* 2013, **2**, 1259–1266
20. M.S. Mannoor, H. Tao, H. Clayton, J.D.A. Sengupta, D.L. Kaplan, R.R. Naik, N. erma, F.G. Omenetto, M.C. McAlpine. *Nat. Commun.* 2012, **3**, 763.
21. T. Mondal, A.K. Bhowmick, R. Krishnamoorti. *J. Mater. Chem.*, 2012, **22**, 22481-22487
22. L. Zhang, P. Dhillon, H. Yan, S. Farmer, R.W. Hancock. *Agents Chemother.* 2000, **44**, 3317–3321
23. M. Kawai, R. Tanaka, H. Yamamura, K. Yasuda, S. Narita, H. Umemoto, S. Ando, T. Katsu, *Chem. Commun.* 2003, 1264-1265.
24. (a) W.S. Hummers, R.E. Offeman. *J. Am. Chem. Soc.*, 1958, **80**, 1339–1339; (b) H.N. Abdelhamid, H.F. Wu. *Anal. Chim. Acta*, 2012, **751**, 94– 104

25. (a) S. Park, J.H. An, I.W. Jung, R.D. Piner, S.J. An, X.S. Li, A. Velamakanni, R.S. Ruoff. *Nano Lett.* 2009, **9**, 1593–1597; (b) F. Kim, L.J. Cote, J.X. Huang. *Adv. Mater.* 2010, **22**, 1954–1958
26. M.C. Wu, A.R. Deokar, J.H. Liao, P.Y. Shih, Y.C. Ling. *ACS Nano*, 2013, **7**, 1281-1290.
27. Y.W. Wang, Y.Y. Fu, L.J. Wu, J. Li, H.H. Yang, G.N. Chen. *J. Mater. Chem. B*, 2013, **1**, 2496-2501.
28. H.F. Wu, J. Gopal, H.N. Abdelhamid, N. Hasan. *Proteomics*. 2012, **12**, 2949–2961.
29. H.N. Abdelhamid , H.F. Wu. *Talanta*, 2013, **115**, 442–450.
30. (a) X. Yang, X. Zhang, Z. Liu, Y. Ma, Y. Huang, Y. Chen. *J. Phys. Chem. C*, 2008, **112**, 17554–17558; (b) X. Yang, Y. Wang, X. Huang, Y. Ma, Y. Huang, R. Yang, H. Duan, Y. Chen. *J. Mater. Chem.*, 2011, **21**, 3448–3454; (c) V.K. Rana, M.C. Choi, J.Y. Kong, G.Y. Kim, M.J. Kim, S.H. Kim, S. Mishra, R.P. Singh, C.S. Ha. *Mater. Eng.*, 2011, **296**, 131–140
31. O.N. Ruiz, K.A.S. Fernando, B. Wang, N.A. Brown, P.G. Luo, N.D. McNamara, M. Vangsness, Y.P. Sun, C.E. Bunker. *ACS Nano*, 2011, **5**, 8100–8107.
32. J. Gopal, H.N. Abdelhamid, P.Y. Hua, H.F. Wu. *J. Mater. Chem. B*, 2013, **1**, 2463-2475.
33. Y. Zhu, M.D. Stoller, W. Cai, A. Velamakanni, R.D. Piner, D. Chen, R.S. Ruoff, *ACS Nano*, 2010, **4**, 1227-1233.
34. H. Pandey, V. Parashar, R. Parashar, R. Prakash, P.W. Ramteke, A.C. Pandey. *Nanoscale*, 2011, **3**, 4104-4108.

35. O. Akhavan, E. Ghaderi, H. Emamy, F. Akhavan, *Carbon* 2013, **54**, 419–431
36. O. Akhavan, E. Ghaderi, A. Akhavan, *Biomaterials*, 2012, **33**, 8017-8025
37. J.R. Lakowicz, *Principle of Fluorescence Spectroscopy*, third ed, Springer Science & Business Media, New York, 2006.
38. W. Hu, C. Peng, M. Lv, X. Li, Y. Zhang, N. Chen, C. Fan, Q. Huang. *ACS Nano*. 2011, **5**, 3693–3700.
39. S. He, B. Song, D. Li, C. Zhu, W. Qi, Y. Wen, L. Wang, S. Song, H. Fang, C.A, A. Fan. *Adv. Funct. Mater.* 2010, **20**, 453–459.
40. X. Zuo, S. He, D. Li, C. Peng, Q. Huang, S. Song, C. Fan. *Langmuir* 2009, **26**, 1936–1939.
41. S. Song, Y. Qin, Y. He, Q. Huang, C. Fan, H. Chen. *Chem. Soc. Rev.* 2010, **39**, 4234–4243.
42. Y.Y. Chang, S.T. Yang, J.H. Liu, E. Dong, Y. Wang, A. Cao, Y. Liu, H. Wang. *Toxicol. Lett.* 2011, **200**, 201–210.
43. Y. Zhang, S.F. Ali, E. Dervishi, Y. Xu, Z. Li, D. Casciano, A.S. Biris. *ACS Nano* 2010, **4**, 3181–3186.
44. O. Akhavan, E. Ghaderi. *Carbon*. 2012, **50**, 1853–1860
45. E.C. Salas, Z. Sun, A. Luttge, J.M. Tour. *ACS Nano* 2010, **4**, 4852–6.
46. G. Wang, F. Qian, C.W. Saltikov, Y. Jiao, Y. Li. *Nano Res* 2011, **4**, 563–70.
47. H. Chen, M.B. Muler, M.J. Gilmore, G. Wallace, D. Li. *Adv. Mater.* 2008, **20**, 3557–3561.
48. S. Agarwal, X. Zhou, F. Ye, Q. He, G.C.K. Chen, J. Soo, F. Boey, H. Zhang, P. Chen. *Langmuir*. 2010, **26**, 2244–2247.

49. S. Liu, M. Hu, T.H. Zeng, R. Wu, R. Jiang, J. Wei, L. Wang, J. Kong, Y. Chen. *Langmuir*. 2012, **28**, 12364–12372.
50. K.M. Garza, K.F. Soto, L.E. Murr. *Int. J. Nanomed.* 2008, **3**, 83–94.
51. K.H. Liao, Y.S. Lin, C.W. MacOsco, C.L. Haynes. *ACS Appl Mater Interfaces*. 2011, **3**, 2607–2615.
52. M. Sawangphruk, P. Srimuk, P. Chiochan, T. Sangsri, P. Siwayaprahm. *Carbon*. 2012, **50**, 5156-5161.
53. H. Ren, C. Wang, J. Zhang, X. Zhou, D. Xu, J. Zheng, S. Guo, J. Zhang. *ACS Nano*. 2011, **4**, 7169–7174.
54. K. Sato, Y. Yamaguchi, U.Nagai, *Bull. Chem. Soc. Jpn.*, 2013, **86**, 112–120
55. Y. Tu, M. Lv, P. Xiu, T. Huynh, M. Zhang, M. Castelli, Z. Liu, Q. Huang, C. Fan, H. Fang, R. Zhou. *Nat. Nanotechnol.* 2013, **8**, 594–601.
56. L. Hui, J.G. Piao, J. Auletta, K. Hu, Y. Zhu, T. Meyer, H. Liu, L. Yang, *ACS Appl. Mater. Interfaces* 2014, **6**, 13183–13190
57. X. Yang, Z. Li, E. Ju, J. Ren, X. Qu, *Chem. Eur. J.* 2014, **20**, 394 – 398
58. H. Bao, Y. Pan, Y. Ping, N. G. Sahoo, T. Wu, L. Li, J. Li, L. H. Gan, *small* 2011, 7, No. 11, 1569–1578
59. B.S. Wu, H.N. Abdelhamid, H.F. Wu. *RSC advances*. 2013, **4**, 3722-3731.

Figure Captions:

Figure 1. Characterization of GO and their derivative (GOGD) using TEM images of (A) GO and (B) GOGD, (C) UV, (D) FTIR, (E) calibration curve using MALDI-MS

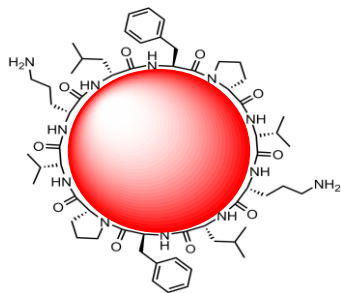
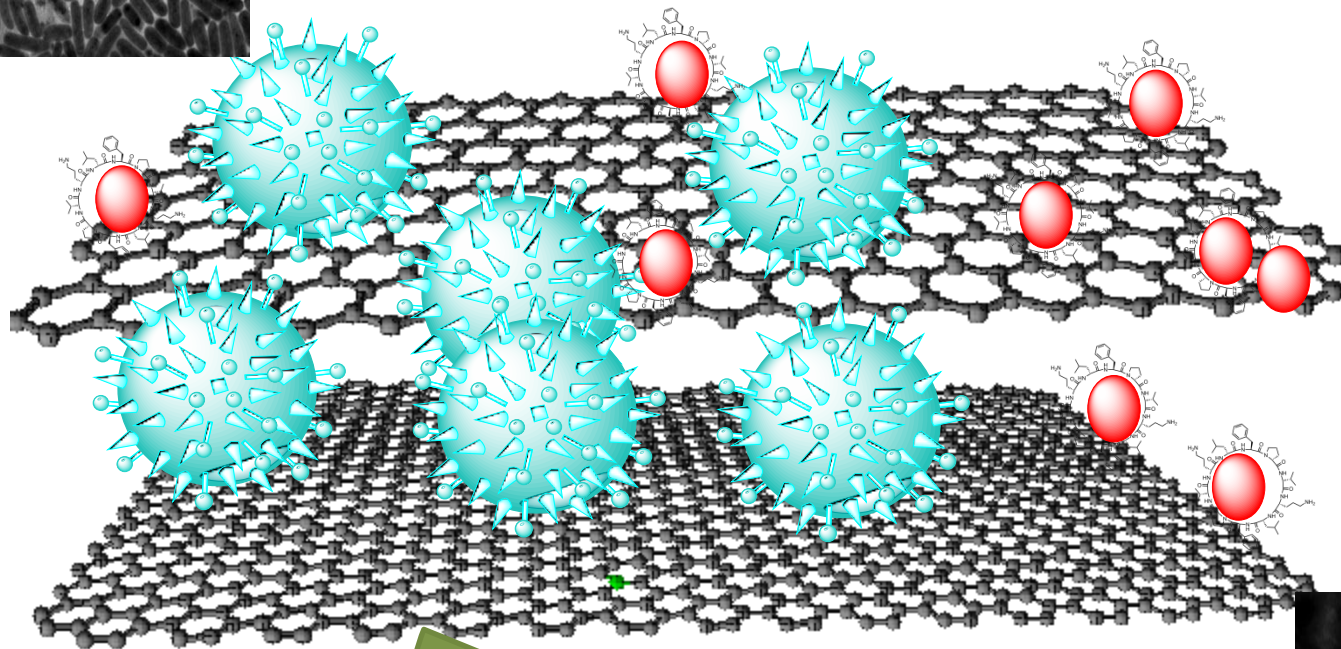
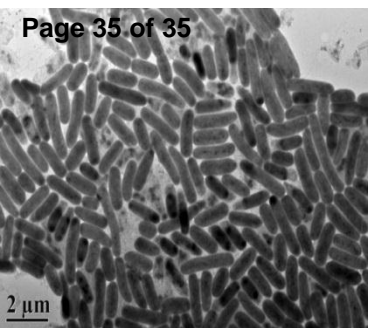
Figure 2. (A) SEM and (B) EDX analysis for GOGD, Biological activity of GD, GO, and GOGD using optical density (OD_{600}) and plate counting. Optical density (OD_{600}) for *P. aeruginosa* (C) and *S. aureus* (D), and plate counting *P. aeruginosa* (E) and *S. aureus* (F)

Figure 3. Fluorescence emission of tryptophan for (A) *P. aeruginosa* and (B) *S. aureus* after incubation with (a) GD, (b) GO and (c) GOGD

Figure 4. 3D-Fluorescence emission of tryptophan for (A) *P. aeruginosa* and (B) *S. aureus* after incubation with (a) control, (b) GD, (c) GO and (d) GOGD

Figure 5. MALDI-MS spectra of (A) *P. aeruginosa* and (B) *S. aureus* after incubation with (a) control, (b),GD (b) GO and (d) GOGD

Figure 6. TEM images of (A) *P. aeruginosa* and (B) *S. aureus* after incubation with (a) control, (b) GD, (c) GO and (d) GOGD



GD

